TECHNISCHE MECHANIK
an open access journal

journal homepage: www.ovgu.de/techmech

Tech. Mech., Vol. 43, Is. 1, (2023), 2–12

Received: 16.02.2023
Accepted: 16.02.2023
Available online: 17.02.2023

Steric Effect Induced Heat Transfer for Electroosmotic Flow of Carreau Fluid through a Wavy Microchannel

Sumit Kumar Mehta[1], Sukumar Pati[1], László Baranyi[2⋆]

[1] Department of Mechanical Engineering, National Institute of Technology Silchar, Silchar, India-788010
[2] Corresponding Author: Department of Fluid and Heat Engineering, Institute of Energy Engineering and Chemical Machinery, University of Miskolc, 3515, Miskolc-Egyetemváros, Hungary

Abstract: We investigate the heat transfer and flow characteristics for an electroosmotic flow of Carreau fluid through a wavy microchannel, considering the finite size of ions i.e., steric effect. The flow of electrolytic liquid is considered steady, two-dimensional and incompressible. The modified Poisson-Boltzmann equation, Laplace equation, continuity equation, momentum equation, and energy equation are solved numerically using a finite element method-based solver. The computed flow and temperature fields are validated by comparison with published results. The flow and temperature fields and average Nusselt number are computed by varying the steric factor, Weissenberg number, dimensionless amplitude and Brinkman number in the following ranges: $0 \leq \nu \leq 0.3$, $0.01 \leq Wi \leq 1$, $0.1 \leq \alpha \leq 0.5$ and $10^{-5} \leq Br \leq 10^{-3}$, respectively. We found the locations of the local maxima and minima of Nusselt number at the convex and concave surfaces of the channel for a lower Brinkman number (=10^{-5}). In contrast, the corresponding locations are swapped at higher Brinkman number (=10^{-3}). The value of average Nusselt number increases with the increase in Weissenberg number and decreases with the steric factor for the smaller Brinkman number (=10^{-5}). Whereas, it decreases with Wi for non-zero values the of steric factor with higher Brinkman number (=10^{-3}). Moreover, the increase in amplitude enhances the average Nusselt number at higher Brinkman number (=10^{-3}).

Keywords: Electroosmosis; heat transfer; steric effect; viscous heating, wavy microchannel.

Nomenclature
Br [-] = Brinkmann number
E^*_{ref} [V/m] = Reference external electric field
G [-] = Joule heating term
H [m] = Inlet half height of microchannel
Nu [-] = Nusselt number
$\overline{Nu}$ [-] = Average Nusselt number
q [W/m^2] = Heat flux
$\mathbf{u}$ [-] = Dimensionless velocity vector
Wi [-] = Weissenberg number
ν [-] = Steric factor
α [-] = Dimensionless amplitude

1 Introduction

In recent times, analysis of transport phenomena in microfluidic channels has received serious attention due to its wide range of engineering applications, such as biomedical and pharmaceutical industries (Mehta et al., 2022a; Mehta and Pati, 2022; Vasista et al., 2022). For microfluidic transport of electrolyte, flow actuated by an external electrical forcing also known as electroosmotic flow (EOF) is one of the suitable flow actuation mechanism widely used due to better flow control and simplicity of the system (Banerjee et al., 2021; Mehta et al., 2021; Mondal et al., 2021; Pabi et al., 2021; Sujith et al., 2021; Vasista et al., 2021a; Vasista et al., 2021b; Zhao et al., 2008). Further, the micro-level heat exchanging systems using EOF is getting significant attention because of its applications in electronics cooling (Eng et al., 2007).

Using wavy surfaces, the fluid-solid interfacial area for heat transfer can be enhanced and accordingly channel with wavy walls is one of the effective methods for heat transfer enhancement (Mehta et al., 2022c; Mehta et al., 2022b; Mehta and Pati, 2020; Pati et al., 2017). Cho et al., (2012) investigated the heat transfer characteristics for the combined electroosmotic and pressure-driven flow through a complex wavy microchannel considering the Joule heating effect. They found that the value of maxima of Nusselt number increases with the increase in the amplitude of the complex wavy wall.

For several microfluidic applications, fluid is non-Newtonian in nature (Mehta et al., 2021). Researchers have developed

⋆ E-mail address: laszlo.baranyi@uni-miskolc.hu
doi: 10.24352/UB.OVGU-2023-040

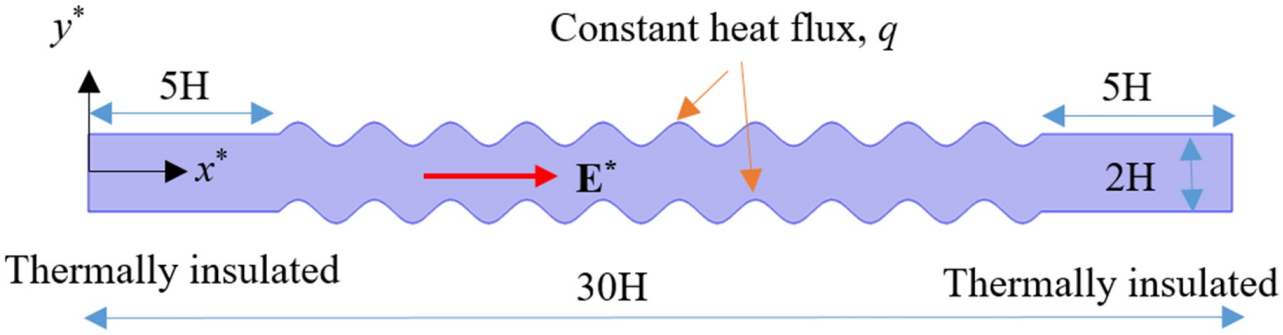

Fig. 1: Physical domain

and employed several models, namely, power-law model (Babaie et al., 2011), Carreau model (Mehta et al., 2021), Casson model (Bag and Bhattacharyya, 2018), moldflow second-order model (Koh et al., 2004) to describe the constitutive behaviour of non-Newtonian fluids. Moghadam (2013) investigated the heat transfer characteristics for electrokinetic-driven flow of non-Newtonian power-law fluid through a circular microtube and found that the trend of fully developed Nusselt number is either increasing or decreasing with the increase in flow behaviour index and the length scale ratio. Noreen et al. (2019) studied the heat transfer characteristics for electroosmotic flow of Carreau fluid through a wavy microchannel and reported that the increase in Weissenberg number increases the Nusselt number.

The classical Poisson-Boltzmann model over-predicts the ionic concentration in electric double-layer (EDL) by neglecting the effect of finite ion size. However, the effect of ions size cannot be ignored for the higher surface charge density. Accordingly, several researchers have used the modified Poisson-Boltzmann equation duly incorporating the effect of finite size of ions by introducing steric factor to find the EDL potential (Fadaei et al., 2022; Liu and Jian, 2019). Dey et al. (2013) investigated the effect of finite size of ions on the heat transfer characteristics for combined electroosmotic and pressure-driven flow through the microchannel. They reported that the point charge assumption overestimates the Nusselt number.

This brief literature survey reveals that no work has been reported investigating the effect of finite size of ions on the heat transfer characteristics for flow of Carreau fluid in a wavy microchannel, which is the main focus of the present work.

2 Theoretical Formulation

We consider an electroosmotic flow of Carreau fluid through a wavy microchannel with inlet half-height, $2H$, as shown in Fig. 1. Both walls of the channel at the inlet and outlet are planar having an axial length of $5H$ each and in the intermediate part having an axial length of $20H$, the walls are wavy, the sinusoidal profiles of which are taken as (Cho et al., 2012; Mehta et al., 2021; Vasista et al., 2021a):

$$\mathrm{S}^*_{Top}(x^*) = H + \alpha H \sin(\pi(x^* - 5H)/H) \tag{1}$$

$$\mathrm{S}^*_{Bottom}(x^*) = -H + \alpha H \sin(\pi(x^* - 5H)/H) \tag{2}$$

The amplitude of the wavy walls is taken as α times of the inlet half-height and the value of α is taken in the range of 0.1 to 0.5 (Cho et al., 2012; Mehta et al., 2021; Vasista et al., 2021a), such that the curvature effect on the ionic distribution can be neglected as the radius of curvature ($(((H_W/4)^2)/A = 0.5H$ to $0.25H$) is large compared to the inlet half-height (Mehta et al., 2021), where is the wavelength. The planar walls are insulated, while the wavy walls are imposed with constant heat flux, q. It is assumed that flow of electrolytic liquid is steady, two-dimensional and incompressible. The temperature-independent thermo-physical properties are taken into consideration. Moreover, the ionic distribution is static as the ionic Peclet number is smaller than unity. The shear rate dependent apparent viscosity of the biofluids that are typically used in microfluidic applications is taken into account in the Carreau model (Mehta et al., 2021). When the temperature is above a critical limit, many reagents lose their effectiveness and alter the molecular functioning of biological systems in such biological fluids (Kunti et al., 2017) inside the heat generating microfluidic system (Peng et al., 2019). Because of changes in chemical structure at the molecular level, a change in temperature has a substantial impact on the stability of the proteins (Somero, 1995). Additionally, temperature change has a significant influence on the activity of the enzymes and aggregation of platelets (Wolberg et al., 2004). For such a microfluidics system, temperature control or heat transfer enhancement analysis is therefore required (Peng et al., 2019). The current model has the above-mentioned specific applications. The governing equations (modified Poisson-Boltzmann equation, Laplace equation, continuity equation, momentum equation and energy equation) in dimensionless form relevant to the present work are as follows (Mehta et al., 2021; Noreen et al., 2019):

$$\nabla^2\psi = \kappa^2 \sinh(\psi)/(1 + (4\nu \sinh^2(\psi/2))) \tag{3}$$

$$\nabla^2\phi = 0 \tag{4}$$

$$\nabla \cdot \mathbf{u} = 0 \tag{5}$$

$$Re(\mathbf{u}\cdot\nabla)\mathbf{u} = -\nabla P + (\nabla\cdot\tau) + (\kappa^2\sinh(\psi)/(1+(4\nu\sinh^2(\psi/2))))\nabla((\psi/\Lambda)+\phi) \tag{6}$$

$$Pe(\mathbf{u}\cdot\nabla\theta) = \nabla^2\theta + Br\Phi + G \tag{7}$$

Here, ψ and ϕ are the dimensionless induced and external potential fields normalized by the scale $\psi^*_{ref} = k_BT/(ze)$ and $\phi^*_{ref} = \Delta VH/(30H)$, respectively; $\mathbf{u} \equiv (u, v)$ is the dimensionless velocity vector normalized by the Helmholtz-Smoluchowski velocity, $u^*_{HS} = -\psi^*_{ref}E^*_{ref}\epsilon/\mu_0$; $\nabla \equiv (x, y)$ is normalized by H ; pressure is normalised by $\mu_0 u^*_{HS}/H$; $\tau = \tau^*(\mu_0 u^*_{HS}/H)^{-1}$ is the dimensionless deviatoric stress tensor, where $\tau^* = \mu(\dot\gamma^*)((\nabla\mathbf{u}^*) + (\nabla\mathbf{u}^*)^T)$; $\dot\gamma^* = \sqrt{0.5(\mathbf{S}:\mathbf{S})}$ is the second invariant of the rate of deformation tensor and $\mathbf{S} = ((\nabla\mathbf{u}^*) + (\nabla\mathbf{u}^*)^T)$ is the strain rate tensor. The apparent viscosity for Carreau fluid can be written as (Mehta et al., 2021):

$$\mu(\dot\gamma^*) = \mu_\infty + (\mu_0 - \mu_\infty)(1 + (\lambda\dot\gamma^*))^{(n-1)/2} \tag{8}$$

where μ_∞ , μ_0 , λ , and n are the infinity and zero shear rate viscosity, relaxation time parameter, and flow behaviour index, respectively. Moreover, the dimensionless temperature is expressed as $\theta = (T - T_{in})/(qH/k)$. Here, $\Phi = (\frac{\partial u}{\partial x}(\tau_{xx} - \tau_{yy}) + (\frac{\partial u}{\partial y} + \frac{\partial v}{\partial x}))$ is the viscous dissipation parameter ;$\tau_{xx} = 2(\overline{\mu_\infty} + (1-\overline{\mu_\infty})(1+(Wi\overline{\dot\gamma}))^{(n-1)/2})\frac{\partial u}{\partial x}$; $\tau_{xy} = 2(\overline{\mu_\infty} + (1-\overline{\mu_\infty})(1+(Wi\overline{\dot\gamma}))^{(n-1)/2})(\frac{\partial u}{\partial y} + \frac{\partial v}{\partial x})$ and $\tau_{yy} = 2(\overline{\mu_\infty} + (1-\overline{\mu_\infty})(1+(Wi\overline{\dot\gamma}))^{(n-1)/2})\frac{\partial v}{\partial y}$ are the components of stresses, where $\dot\gamma = \sqrt{2(\frac{\partial u}{\partial x})^2 + (\frac{\partial u}{\partial y} + \frac{\partial v}{\partial x})^2 + 2(\frac{\partial v}{\partial y})^2}$ (Noreen et al., 2019). Here, $\overline{\mu_\infty}$ is defined as $\overline{\mu_\infty} = \mu_\infty/\mu_0$ the value of which is taken as 0.0616 (Mehta et al., 2021). Here, ν , $\kappa(= H/\lambda_D)$ and $Re(= \rho H u^*_{HS}/\mu_0)$ are the steric factor, Debye parameter, Reynolds number, respectively; $Wi(= \lambda u^*_{HS}/H)$, $\Lambda(= \phi^*_{ref}/\psi^*_{ref})$, and $Pe(= \rho c_p H u^*_{HS}/k)$ are the Weissenberg number, ratio of reference applied to EDL potential, thermal Peclet number, respectively; $Br(= \mu_0(u^*_{HS}/H)^2H/q)$, and $G(= \sigma(E^*_{ref})^2H/q)$ are the Brinkman number, and Joule heating parameter, respectively. Note that $\lambda_D(= ((2n_oz^2e^2)/(\epsilon k_BT))^{-0.5})$, ΔV , ρ , c_p , k , ϵ , $E^*_{ref}(= \Delta V/30H)$, n_o , T and σ are the Debye length, applied external potential difference, density, specific heat capacity, thermal conductivity, electrical permittivity of the liquid, reference external electric field, bulk ionic concentration, reference absolute temperature, and electrical conductivity of the liquid, respectively. The employed boundary conditions are as follows:
At inlet:

$$\mathbf{n}\cdot(\nabla\psi) = 0, \phi = 30, P = P_{atm}, \theta = 0 \tag{9}$$

At wavy walls:

$$\psi = \zeta = 4, \mathbf{n}\cdot(\nabla\phi) = 0, \mathbf{u} = 0, \frac{\partial\theta}{\partial n} = 1 \tag{10}$$

At planar walls:

$$\psi = \zeta = 4, \mathbf{n}\cdot(\nabla\phi) = 0, \mathbf{u} = 0, \frac{\partial\theta}{\partial n} = 0 \tag{11}$$

At outlet:

$$\mathbf{n}\cdot(\nabla\psi) = 0, \phi = 30, P = P_{atm}, \frac{\partial\theta}{\partial x} = 0 \tag{12}$$

Here, $\mathbf{n}$ is the unit vector normal to wavy wall. The heat transfer rate is presented in terms of local Nusselt number (Nu) as (Banerjee et al., 2021; Pabi et al., 2021):

$$Nu = 1/(\theta_{wall} - \theta_{mean}) \tag{13}$$

Here, $\theta_{mean}(= \int_{y_1}^{y_2}(u\theta)\,dy/\int_{y_1}^{y_2}(u)\,dy)$ is the bulk mean temperature of the fluid (Banerjee et al., 2021).
The average Nusselt number ($\overline{Nu}$) is calculated as (Mehta et al., 2022c; Mehta et al., 2022b; Mehta and Pati, 2021):

$$\overline{Nu}=0.5(((\int_{x=5}^{x=25}(Nu)\,dS)/(\int_{x=5}^{x=25}dS))_{Top} + ((\int_{x=5}^{x=25}(Nu)\,dS)/(\int_{x=5}^{x=25}dS))_{Bottom}) \tag{14}$$

Here S is the normalised axial length of the wavy walls.

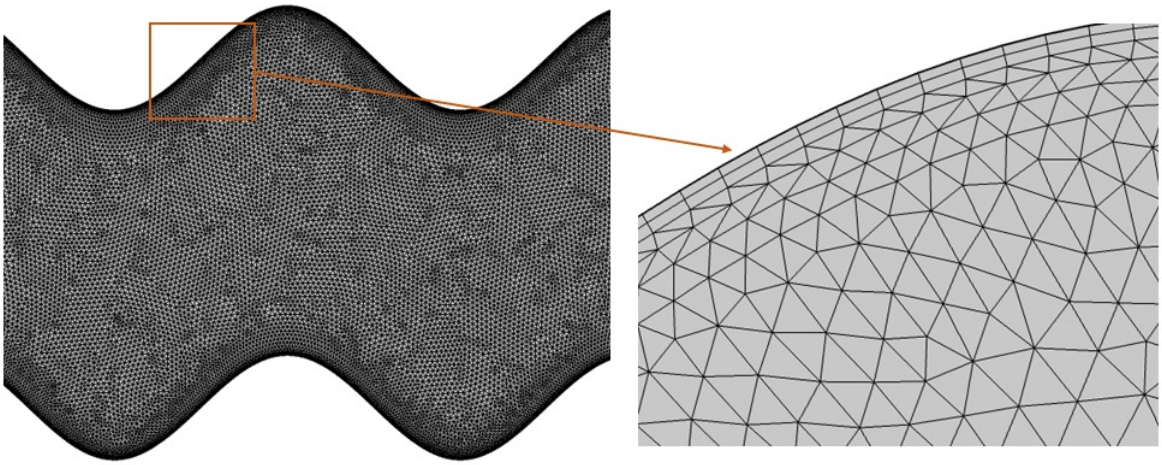

Fig. 2: Grid distribution in wavy microchannel.

3 Numerical Methodology and Model Benchmarking

We employ a finite element method based numerical solver to obtain the flow and temperature fields. The computational domain is divided into large number of small sub-domains in non-uniform manner with denser mesh near the walls. The mesh used for the present computational investigation is presented in Fig. 2. Using Galerkin weighted method, the governing equations are first discretised and then the resulting equations are solved iteratively until the pre-defined residual value of 10^{-6} is reached. An exhaustive grid independence test was performed by calculating the average Nusselt number as depicted in Table 1; the relative difference of the value for the mesh system with 130144 elements and the next level finer mesh was less than 1%. Accordingly, the mesh with 130144 elements was used for all the simulations.

We validate the solver by comparing the electroosmotic flow velocity profile with the results of Zhao et al. (2008) for parallel plate channel shown in Fig. 3(a) for n=1, κ=10, ν=0 and $\zeta = 1$. A second validation was done with the experimental results of Tang et al. (2006) for electroosmotic flow through a plane microchannel having 200 µm height, as illustrated in Fig. 3(b). This validation was done for the limiting case $n = 1$ and $\nu = 0$ for 10^{-4}M $NaHCO_3$ – water solution with electric field intensity 60000 V/m, and zeta potential, -75 mV. The next validation is presented in Fig. 3(c) by comparing the dimensionless wall temperature for EOF in a plane microchannel with the results of Horiuchi and Dutta (2004). For this validation, the values of different parameters considered are as follows: Pe=100, κ=100, Br=0, n=1 and ν=0. Further, the comparison of the average Nusselt number with change in $1/\kappa$ for a long plane microchannel with the analytical result of Sadeghi et al. (2011) is shown in Fig. 3(d) for the limiting case n =1, $G = 1$, $Br = 0$, $\zeta = 1$, $Pe = 1$ and $\nu = 0$. The comparisons show a good agreement of the present result with the published works (Horiuchi and Dutta, 2004; Zhao et al., 2008; Tang et al., 2006; Sadeghi et al., 2011).

4 Results and Discussion

We analyse the heat transfer and flow characteristics for an ionic size dependent electroosmotic flow of Carreau fluid through a wavy microchannel. The results are presented in terms of flow and temperature fields, local Nusselt number (Nu) and average Nusselt number ($\overline{Nu}$) by varying the steric factor (ν), Weissenberg number (Wi), Brinkman number (Br) and dimensionless amplitude (α) in the range of $0 \leq \nu \leq 0.3$, $0.01 \leq Wi \leq 1$, (Hayat et al., 2010; Mehta et al., 2021; Noreen et al., 2019), $10^{-5} \leq Br \leq 10^{-3}$ (Pabi et al., 2021; Zhao et al., 2008; Sujith et al., 2022)) and $0.1 \leq \alpha \leq 0.5$ (Cho et al., 2012; Mehta et al., 2021; Vasista et al., 2021a), respectively The value of n and Re is kept fixed at 0.4 and 0.001, respectively (Hayat et al., 2010; Mehta et al., 2021).

Figure 4 shows the transverse variation of dimensionless flow velocity at x=10.5 for different values of Wi and ν. It is observed that the increase in ν from 0 to 0.3 decreases the flow velocity due to the increase in flow resistance caused by the electrostatic pull inside the EDL by the finite size of ions (Mehta et al., 2021). It is also seen that the decrement is higher near the

Tab. 1: Grid independence test at different mesh system (M) calculating average Nusselt number when ν =0.3, n=0.4, Wi=1, Br=10-3 and κ=30.

Mesh type	Number of elements	Average Nusselt number ($\overline{Nu}$)	Percentage difference w. r. t. M4
M1	20206	3.5294	24.586
M2	51869	3.0219	6.671
M3	130144	2.8376	0.166
M4	218108	2.8329	0

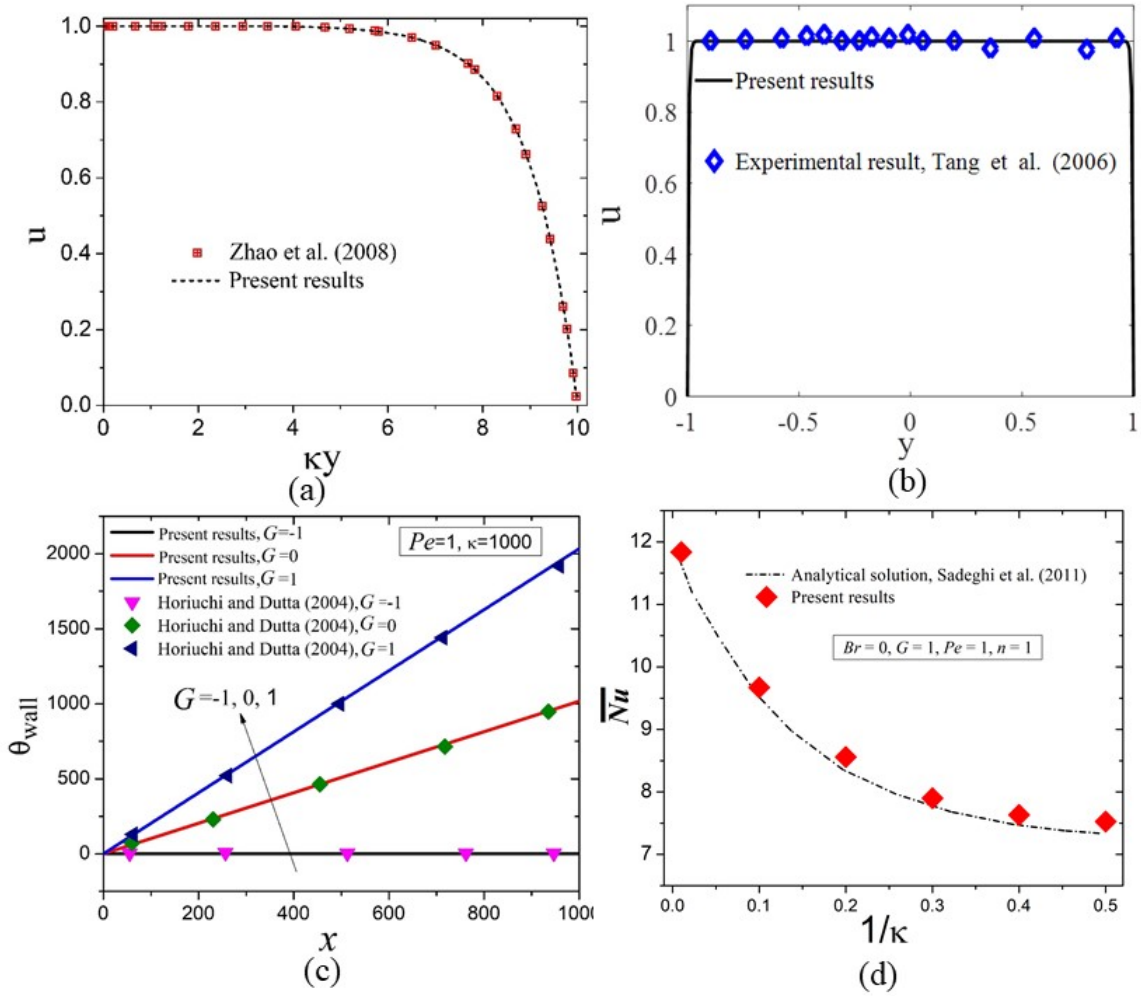

Fig. 3: Comparison of (a) dimensionless electroosmotic flow velocity in a parallel plate channel κ=10, ν=0 and ζ = 1 at the limiting case, n=1, (b) dimensionless electroosmotic flow velocity with the experimental results of Tang et al.(2006) at limiting case, n = 1 and ν = 0 for 10^{-4} M $NaHCO_3$ –water solution with electric field intensity 60,000 V/m, and zeta potential, -75mV for flow through plane microchannel, (c) non-dimensional wall temperature for EOF through a plane microchannel for different G values with the results of Horiuchi and Dutta (2004) for Pe=100, κ = 100, Br=0, n = 1, ζ = 1 and ν = 0, (d) average Nusselt number with 1/κ for long plane microchannel with the analytical results of Sadeghi et al. (2011) for limiting case of n =1, G = 1, Br = 0, ζ = 1, Pe = 1 and ν = 0.

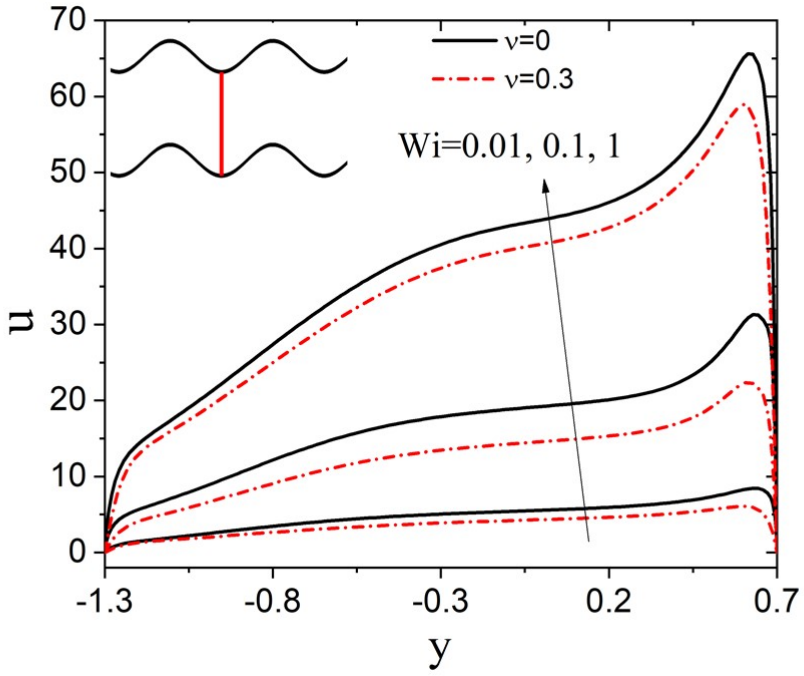

Fig. 4: Variation of transverse dimensionless velocity profile at x=10.5 for different values of steric factor and Wi.

walls as the flow resistance is only within the EDL. Furthermore, the flow velocity at any transverse location increases as Wi increases which is attributed to the decreases in apparent viscosity of the fluid.

The streamlines and dimensionless flow velocity contours at different Wi are presented in Fig. 5 at ν=0.3. It is observed that the streamlines near the wall follow the profile of the wavy walls and accordingly they become a wavy. Further, the minima and maxima of velocity exist near the concave and convex surfaces due to the smaller and higher electric field intensity, respectively. Moreover, the flow velocity is enhanced with Wi due to the decrease in the apparent viscosity of the fluid.

Figure 6(a) and (b) show the contours of dimensionless isotherms at different Wi and Br for ν=0 and 0.3, respectively. It is seen that the increase in Wi from 0.01 to 1 decreases the temperature in the domain due to the increase in convective heat transfer (see Fig. 4). Further, the decrease in convection strength with the increase in steric factor from 0 to 0.3 (see Fig. 4) increases the isotherms values for ν=0.3 compared to ν=0. It is also noted that the increase in Br augments the temperature of fluid due to the increase in viscous dissipation effect. The increment is significantly higher for the higher Wi (=1) values, which is attributed to the higher velocity gradient (see Fig. 4).

Figure 7(a) and (b) shows the variation of local Nusselt number (Nu) at the top wall for different ν values with Br=10^{-5} and 10^{-3} at Wi=1. It is observed that the locations of the local maxima and minima of Nu are at the convex and concave surfaces, respectively due to higher and smaller velocity gradient for the smaller Br (=10^{-5}). In contrast, these minima and maxima locations are shifted to convex and concave surface, respectively at Br =10^{-3} . It is attributed to the higher velocity near the convex surface causing very high viscous dissipation effect at higher Br. Furthermore, the increase in ν decreases the value of Nu for Br = 10^{-5} and the trend is opposite for Br =10^{-3}. These observations can be explained as follows. For smaller Br (=10^{-5}) values the significant increase in wall temperature compared to the core temperature (see Fig. 6) due to the decrease in flow velocity (see Fig. 4) increases the difference of $(\theta_{wall} - \theta_{mean})$ with ν. Whereas, for higher Br (=10^{-3}), the decrease in velocity gradient with ν (see Fig. 4) near the walls significantly reduces the viscous heating and augments the heat transfer rate with ν.

The variation of average Nusselt number ($\overline{Nu}$) with Wi for different ν values is shown in Fig. 8(a) and (b) for Br=10^{-5} and 10^{-3}, respectively. It is observed that the value of $\overline{Nu}$ increases with Wi for Br =10^{-5}. This is attributed to the fact that the increase in flow velocity with Wi (see Fig. 4) significantly reduces the wall temperature compared to the bulk temperature and the decrease in $(\theta_{wall} - \theta_{mean})$ with Wi increases the value of $\overline{Nu}$. Also, it is seen in Fig. 8(a) that $\overline{Nu}$ decreases with for smaller (Br =10^{-5})

Tab. 2: Percentage change in average Nusselt number $(100((\overline{Nu}_{\nu=0}) - (\overline{Nu}_{\nu\neq0}))/(\overline{Nu}_{\nu=0}))$ for ν =0.3 compared to the case when ν=0.

Wi	0.01	0.025	0.05	0.075	0.1	0.3	0.5	0.7	0.9	1
Br=10^{-5}	6.19	13.27	18.361	20.10	20.92	22.35	22.83	23.16	23.39	23.49
Br=10^{-3}	-31.04	-66.35	-84.02	-84.44	-80.32	-56.70	-48.28	-44.02	-41.4	-40.51

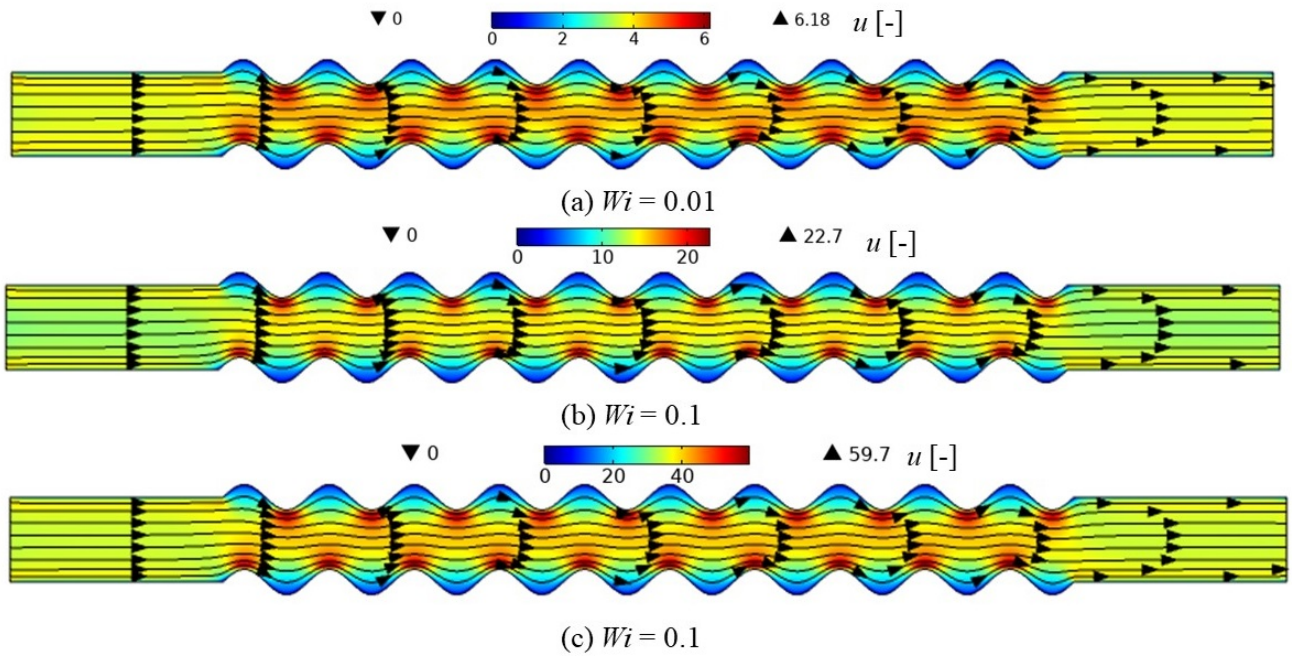

Fig. 5: Streamlines and dimensionless flow velocity contours at different Wi for ν =0.3, n=0.4 and κ=30.

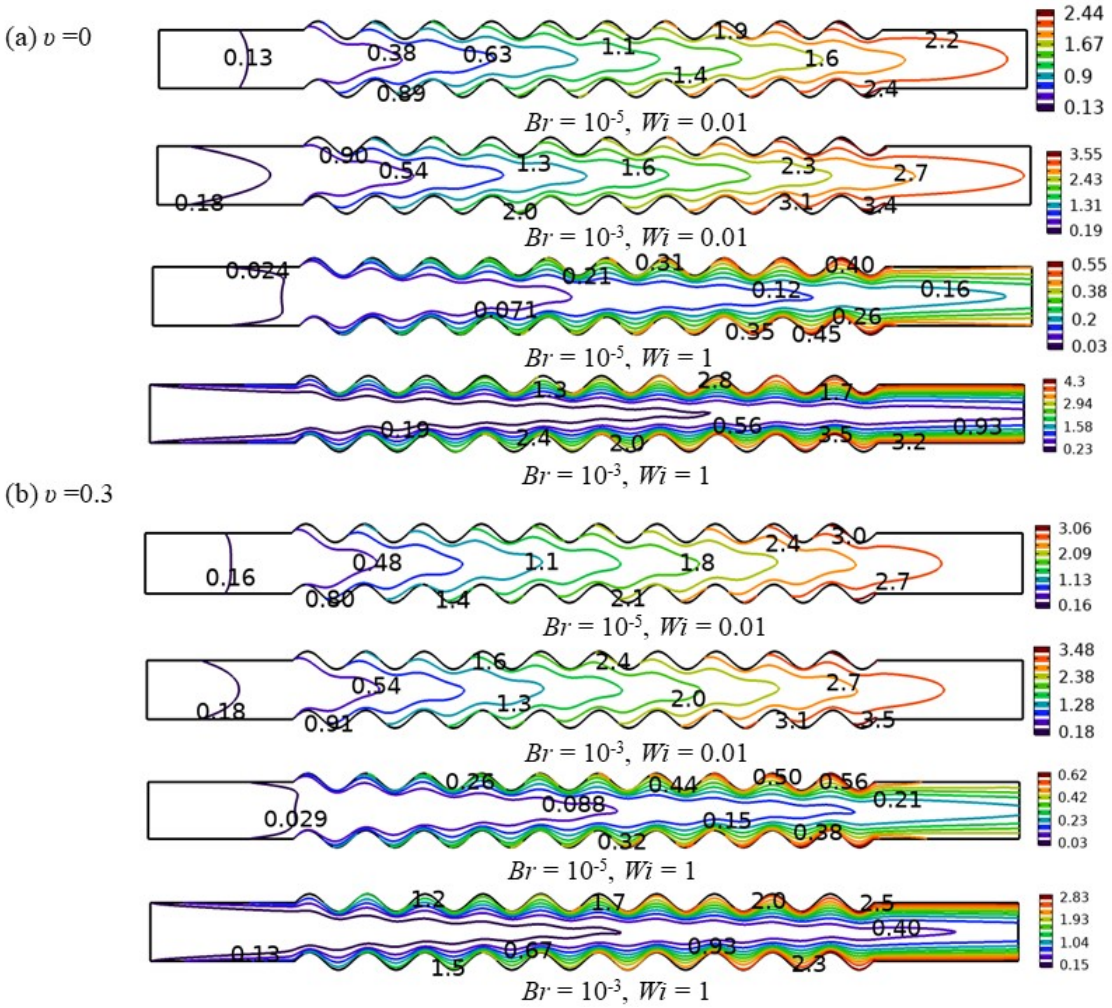

Fig. 6: Contours of dimensionless isotherms for different Br and Wi values at (a) ν=0 and (b) ν=0.3, when ζ=4, κ=30, Pe=5, n=0.4 and G=1. The colour legends represent the dimensionless temperature, θ.

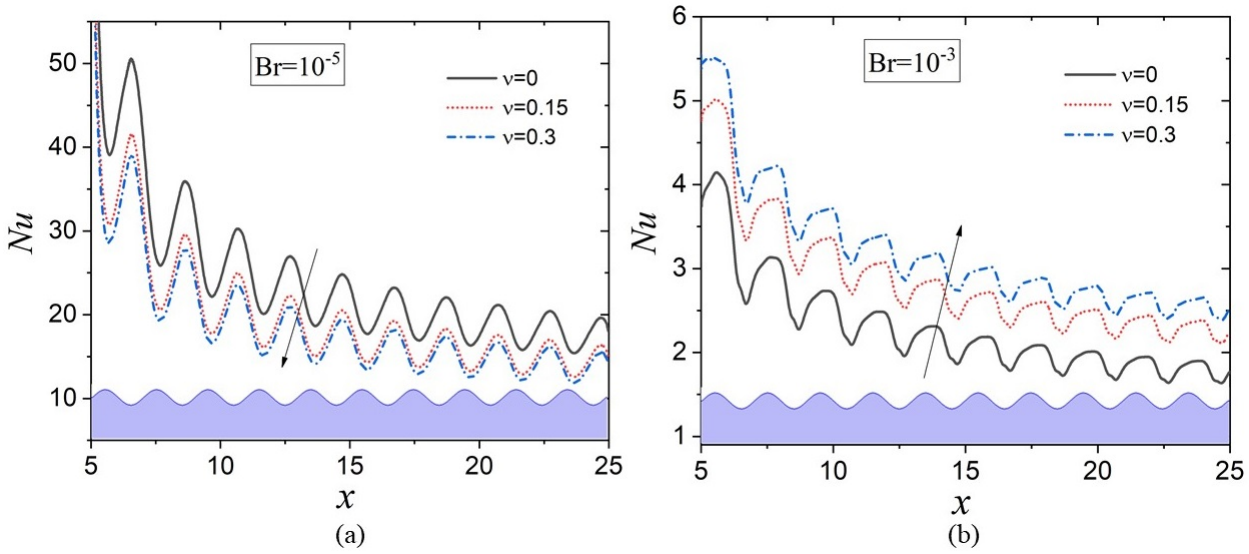

Fig. 7: Variation of local Nusselt number at different ν values for (a) Br=10^{-5} and (b) Br=10^{-3} when ζ=4, κ=30, Pe=5, n=0.4 and G=1.

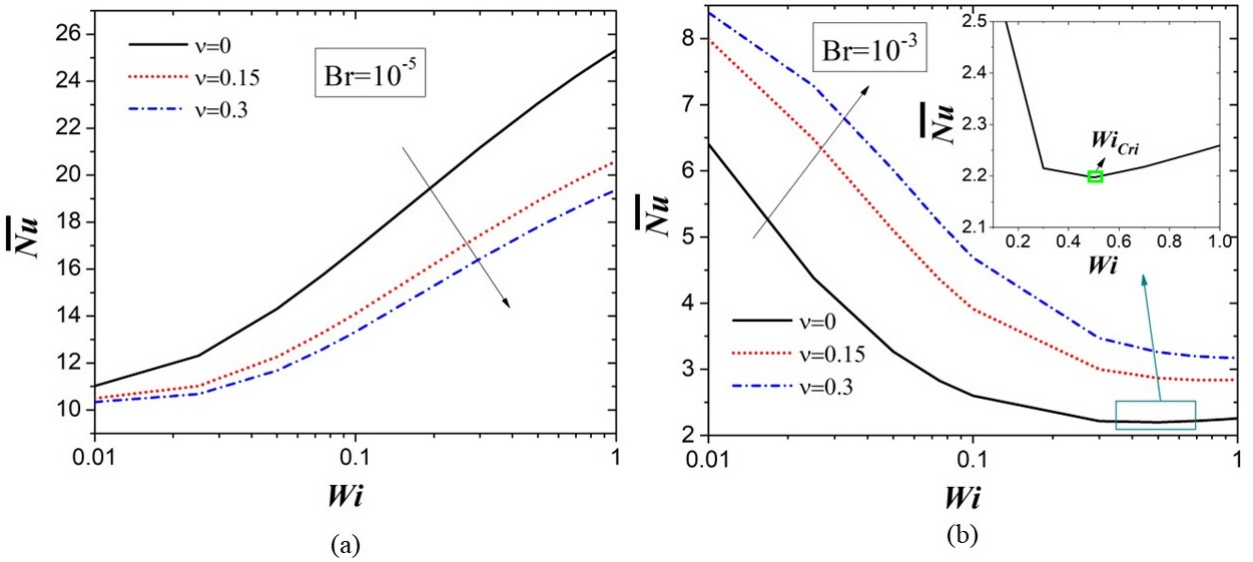

Fig. 8: Variation of average Nusselt number with Wi at different ν values for (a) Br=10^{-5} and (b) Br=10^{-3} when ζ=4, κ=30, Pe=5, n=0.4 and G=1.

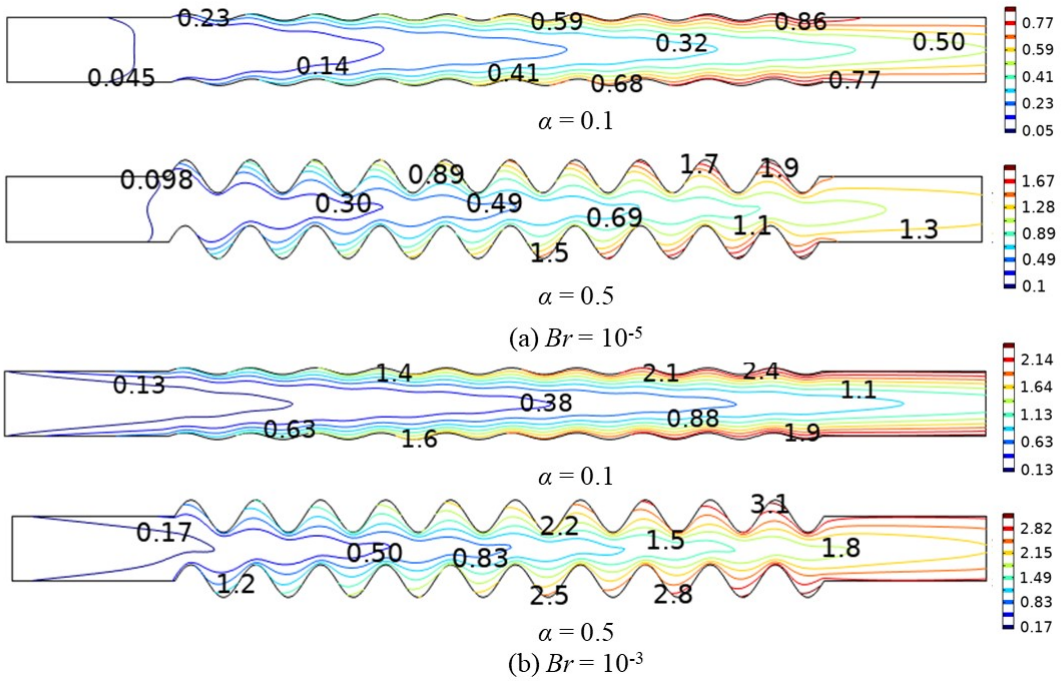

Fig. 9: Contours of dimensionless isotherms for different wave amplitudes for (a) Br=10^{-5} and (b) Br=10^{-3}at ζ=4, ζ=30, Pe=5, n=0.4, Wi=0.1, ν=0.3 and G=1. The colour legends represent the dimensionless temperature, θ.

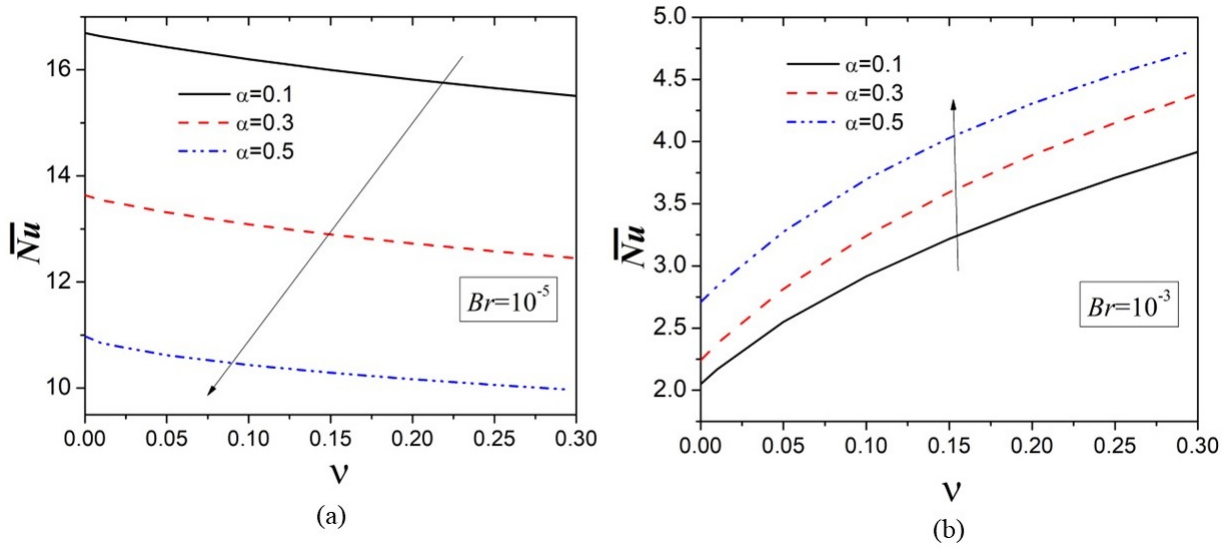

Fig. 10: Variation of average Nusselt number with ν at different dimensionless amplitudes of wavy wall α for (a) Br=10^{-5} and (b) Br=10^{-3} at ζ=4, κ=30, Pe=5, n=0.4, Wi=0.1 and G=1

which can be explained from the variation of local Nusselt number with ν. The value of $\overline{Nu}$ decreases with Wi for ν=0.15 and 0.3, and it follows the increasing-decreasing trend with Wi for the point charge case (ν=0), and a critical Wi (Wi_{Cri}) is found for Br =10^{-3}. The decrease in $\overline{Nu}$ with Wi is attributed to the augmentation in viscous heating (see Fig. 4), which decreases the heat transfer rate. Whereas, for higher Wi values ($> Wi_{Cri}$), the enhanced convective strength decreases the core region temperature and hence the value of ($\theta_{wall} - \theta_{mean}$). Furthermore, it is seen in Fig. 8(b) that the value of $\overline{Nu}$ increases with which can be explained from the variation of local Nusselt number. The values of the decrease and increase in $\overline{Nu}$ are obtained as 23.49% and 40.51% for change in ν from 0 to 0.3 for Br=10^{-5} and 10^{-3}, respectively, as shown in Table 2 when Wi=1. Moreover, the maximum under-prediction in average Nusselt number is obtained as 84.44 % when Br =10^{-3} at Wi=0.075 as found from Table 2.

Figure 9(a) and (b) show the contours of dimensionless isotherms at different dimensionless amplitude of wavy wall α and Br when ν= 0.3. It can be seen that the increase in amplitude of wavy wall causes hot spots near the walls; more towards the upstream for higher α. This is because of the increase in effective heated surface area at higher amplitude. It can also be seen that the increase in amplitude increases the intensity of electroosmotic actuation at the convex section, which leads to an increase in viscous dissipation, as the velocity gradient enhances at the convex section. Therefore, with an increase in amplitude at higher Br, this impact significantly contributes to an increase in domain temperature.

Further, we compare $\overline{Nu}$ with the change in dimensionless wave amplitude α with ν at lower (Br=10^{-5}) and a higher Br (=10^{-3}) values as depicted in Fig. 10(a) and (b), respectively. It is found that the increase in α reduces the value of $\overline{Nu}$ at the smaller Br values. It is attributed to the higher effective surface area for the higher causes more heated wavy walls at the same section compared to smaller α (see Fig. 9(a)). Therefore, the higher wall temperature in the upstream region for higher α leads to an increase in ($\theta_{wall} - \theta_{mean}$). Hence, decreases with α at smaller Br as shown in Fig. 10(a). Moreover, for higher Br, the value of $\overline{Nu}$ increases with α. It can be explained as follows. For higher Br, the significant viscous heating causes considerable heat generation leading to an increase in the core region temperature (see Fig. 9(b)). Moreover, the increase in amplitude leads to higher velocity gradient near the convex section as electroosmotic actuation is stronger by higher external electric field strength (Mehta et al., 2021). Therefore, the increase in amplitude leads to higher bulk temperature (see Fig. 9(b)). The dominancy of increase in bulk mean temperature with α leads to decrease in ($\theta_{wall} - \theta_{mean}$). Hence, $\overline{Nu}$ increases with α at higher Br values as shown in Fig. 10(b). Further, the effect of ν at different α values is the same as discussed for Fig. 8.

5 Conclusions

In the present study, we investigate the heat transfer and flow characteristics for an ionic size dependent electroosmotic flow of non-Newtonian Carreau fluid through a wavy microchannel. The results are presented in terms of flow and temperature fields, local Nusselt number (Nu) and average Nusselt number ($\overline{Nu}$) by varying the steric factor (ν), Weissenberg number (Wi) and Brinkman number (Br) in the following range: $0 \leq \nu \leq 0.3$, $0.01 \leq Wi \leq 1$, and $10^{-5} \leq Br \leq 10^{-3}$. The important sufindings are mmarised as follows:

- The flow velocity increases with Wi and decreases with ν.
- The locations of the local maxima and minima of Nusselt number are at the convex and concave surfaces for smaller Br (=10^{-5}). In contrast, the locations are swapped at higher Br (=10^{-3}).
- The value of $\overline{Nu}$ increases with Wi and decreases with ν for smaller Br (=10^{-5}) values. Whereas the value of $\overline{Nu}$ decreases with Wi for ν =0.15 and 0.3, and it follows the increasing-decreasing trend with Wi for point charge case (ν =0), and a critical Wi is found for higher Br (=10^{-3}). Moreover, $\overline{Nu}$ increases with ν for higher Br (=10^{-3}).
- The values of the decrease and increase in $\overline{Nu}$ are obtained as 23.49% and 40.51% for the change in ν from 0 to 0.3 for Br=10^{-5} and Br=10^{-3}, respectively, when Wi=1.
- The increase in wavy wall amplitude augments $\overline{Nu}$ at higher Br values while the effect is opposite at smaller Br values.

References

Babaie, A.; Sadeghi, A.; Saidi, M. H.: Combined electroosmotically and pressure driven flow of power-law fluids in a slit microchannel. *J. Non-Newton. Fluid*, 166(14), (2011), 792-798.

Bag, N.; Bhattacharyya, S.: Electroosmotic flow of a non-Newtonian fluid in a microchannel with heterogeneous surface potential. *J. Non-Newton. Fluid*, 259, (2018), 48-60.

Banerjee, D.; Mehta, S. K.; Pati, S.; Biswas, P.: Analytical solution to heat transfer for mixed electroosmotic and pressure-driven flow through a microchannel with slip-dependent zeta potential. *Int. J. Heat Mass Tran.*, 181, (2021), 121989

Cho, C. C.; Chen, C. L.; Chen, C. K.: Characteristics of combined electroosmotic flow and pressure-driven flow in microchannels with complex-wavy surfaces. *Int. J. Therm. Sci.,* 61, (2012), 94-105.

Dey, R.; Ghonge, T.; Chakraborty, S.: Steric-effect-induced alteration of thermal transport phenomenon for mixed electroosmotic and pressure driven flows through narrow confinements. *Int. J. Heat Mass Tran.*, 6(1), (2013), 251-262.

Eng, P. F.; Nithiarasu, P.; Arnold, A. K.; Igic; P.; Guy, O. J.: Electro-osmotic flow based cooling system for microprocessors. *2007 International Conference on Thermal, Mechanical and Multi-Physics Simulation Experiments in Microelectronics and Micro-Systems. EuroSime 2007*, 1-5.

Fadaei, P.; Niazmand, H.; Raoufi, M. A.: Influence of finite size of ions on thermal transport of a simultaneous electrokinetic-pressure driven flow of power-law fluids in a slit microchannel. *Colloid. Surface. A*, 634, (2022), 127857

Hayat, T.; Saleem, N.; Ali, N.: Effect of induced magnetic field on peristaltic transport of a Carreau fluid. *Comm. Nonlinear Sci. Numer. Simul.*, 15(9), (2010), 2407-2423.
Horiuchi, K.; Dutta, P.: Joule heating effects in electroosmotically driven microchannel flows. *Int. J. Heat Mass Tran.*, 47(14), (2004), 3085-3095.
Koh, Y. H.; Ong, N. S.; Chen, X. Y.; Lam, Y. C.; Chai, J. C.: Effect of temperature and inlet velocity on the flow of a non-Newtonian fluid. *Int. Commun. Heat Mass Tran.*, 31(7), (2004), 1005-1013.
Kunti, G.; Bhattacharya, A.; Chakraborty, S.: Analysis of micromixing of non-Newtonian fluids driven by alternating current electrothermal flow, *J. Non-Newton. Fluid*, 247 (2017), 123-131.
Liu, Y.; Jian, Y.: The effects of finitei ionic sizes and wall slip on entropy generation in electroosmotic flows in a soft nanochannel. *J. Heat Transf.*, 141(10), (2019), 102401
Mehta, S. K.; Mondal; B.; Pati, S.; Patowari, P. K.: Enhanced electroosmotic mixing of non-Newtonian fluids in a heterogeneous surface charged micromixer with obstacles. *Colloid. Surface. A*, 648, (2022a), 129215
Mehta, S. K.; Pati, S.: Numerical study of thermo-hydraulic characteristics for forced convective flow through wavy channel at different Prandtl numbers. *J. Therm. Anal. Calorim.*, 141(6), (2020), 2429-2451.
Mehta, S. K.; Pati, S.: Thermo-hydraulic and entropy generation analysis for magnetohydrodynamic pressure driven flow of nanofluid through an asymmetric wavy channel. *Int. J. Numer. Method. H.*, 31(4), (2021), 1190-1213.
Mehta, S. K.; Pati, S.: Enhanced electroosmotic mixing in a wavy micromixer using surface charge heterogeneity. *Ind. Eng. Chem. Res.*, 61(7), (2022), 2904-2914.
Mehta, S. K.; Pati; S.; Ahmed, S.; Bhattacharyya, P.; Bordoloi, J. J.: Analysis of thermo-hydraulic and entropy generation characteristics for flow through ribbed-wavy channel. *Int. J. Numer. Method. H.*, 32(5), (2022b), 1618-1642.
Mehta, S. K.; Pati, S.; Baranyi, L.: Effect of amplitude of walls on thermal and hydrodynamic characteristics of laminar flow through an asymmetric wavy channel. *Case Stud. Therm. Eng.*, 31 (2022c), 101796
Mehta, S. K.; Pati, S.; Mondal, P. K.: Numerical study of the vortex-induced electroosmotic mixing of non-Newtonian biofluids in a nonuniformly charged wavy microchannel: Effect of finite ion size. *Electrophoresis*, 42 (23), (2021), 2498-2510.
Moghadam, A. J.: Electrokinetic-driven flow and heat transfer of a non-Newtonian fluid in a circular microchannel. *J. Heat Transf.*, 135 (2), (2013), 021705
Mondal, B.; Mehta, S. K.; Pati, S.; Patowari, P. K.: Numerical analysis of electroosmotic mixing in a heterogeneous charged micromixer with obstacles. *Chem. Eng. Process.*, 168, (2021) 108585
Noreen, S.; Waheed, S.; Hussanan, A.; Lu, D.: Analytical solution for heat transfer in electroosmotic flow of a Carreau fluid in a wavy microchannel. *Appl. Sci.*, 9(20), (2019), 4359
Pabi, S.; Mehta, S. K.; Pati, S.: Analysis of thermal transport and entropy generation characteristics for electroosmotic flow through a hydrophobic microchannel considering viscoelectric effect. *Int. Commun. Heat Mass Tran.*, 127, (2021), 105519
Pati, S.; Mehta, S. K.; Borah, A.: Numerical investigation of thermo-hydraulic transport characteristics in wavy channels: Comparison between raccoon and serpentine channels. *Int. Commun. Heat Mass Tran.*, 88, (2017). 171-176.
Peng, J.; Fang, C.; Ren, S.; Pan, J.; Jia, Y.; Shu, Z.; Gao, D.: Development of a microfluidic device with precise on-chip temperature control by integrated cooling and heating components for single cell-based analysis, *Int. J. Heat Mass Tran*., 130 (2019), 660–667.
Sadeghi, A.; Fattahi, M.; Saidi, M. H.: An approximate analytical solution for electro-osmotic flow of power-law fluids in a planar microchannel, *J. Heat Transf.*, 133(9), (2011) 091701.
Somero, G. N.: Proteins and temperature, *Annu. Rev. Physiol.*, 57:1 (1995), 43-68.
Sujith, T.; Mehta S. K.; Pati, S.: Effect of non-uniform heating on electroosmotic flow through microchannel. In *Recent Advances in Mechanical Engineering,* Pandey, K. M., Misra, R. D., Patowari, P. K. and Dixit, U.S. (Eds.), Springer Singapore, Singapore, (2021), 499-508.
Sujith, T.; Mehta, S. K.; Pati, S.: Effect of finite size of ions on entropy generation characteristics for electroosmotic flow through microchannel considering interfacial slip. *J Therm. Anal. Calorim.*, (2022). https://doi.org/10.1007/s10973-022-11731-8
Tang, G.; Yan, D.; Yang, C.; Gong, H.; Chai, J. C.; Lam, Y. C.: Assessment of Joule heating and its effects on electroosmotic flow and electrophoretic transport of solutes in microfluidic channels. *Electrophoresis*, 27, (2006), 628-639.
Vasista, K. N.; Mehta, S. K.; Pati, S.: Numerical assessment of hydrodynamic and mixing characteristics for mixed electroosmotic and pressure-driven flow through a wavy microchannel with patchwise surface heterogeneity. *P. I. Mech. Eng. E-J. Pro.*, (2021a). https://doi.org/10.1177/09544089211051640
Vasista, K. N.; Mehta, S. K.; Pati, S.: Electroosmotic mixing in a microchannel with heterogeneous slip dependent zeta potential. *Chem. Eng. Process.*, 176, (2022), 108940
Vasista, K. N.; Mehta, S. K.; Pati, S.; Sarkar, S. (2021), Electroosmotic flow of viscoelastic fluid through a microchannel with slip-dependent zeta potential. *Phys. Fluids*, 33(12), (2021b), 123110
Wolberg, A. S.; Meng, Z. H.; Monroe, D. M.; Hoffman, M.: A systematic evaluation of the effect of temperature on coagulation enzyme activity and platelet function. *J. Trauma,* 56(6) (2004), 1221-1228.
Zhao, C.; Zholkovskij, E.; Masliyah, J. H.; Yang, C.: Analysis of electroosmotic flow of power-law fluids in a slit microchannel. *J. Colloid Interf. Sci.*, 326(2), (2008), 503-510.